



HHS Public Access

Author manuscript

Toxicol Appl Pharmacol. Author manuscript; available in PMC 2015 December 31.

Published in final edited form as:

Toxicol Appl Pharmacol. 2012 August 1; 262(3): 255–264. doi:10.1016/j.taap.2012.05.005.

Induction of pulmonary fibrosis by cerium oxide nanoparticles

Jane Y. Ma^{a,*}, Robert R. Mercer^a, Mark Barger^a, Diane Schwegler-Berry^a, James Scabilloni^a, Joseph K. Ma^b, and Vincent Castranova^a

^aHealth Effects Laboratory Division, National Institute for Occupational Safety and Health, Morgantown, WV 26505, USA

^bSchool of Pharmacy, West Virginia University, Morgantown, WV 26506, USA

Abstract

Cerium compounds have been used as a diesel engine catalyst to lower the mass of diesel exhaust particles, but are emitted as cerium oxide (CeO₂) nanoparticles in the diesel exhaust. In a previous study, we have demonstrated a wide range of CeO₂-induced lung responses including sustained pulmonary inflammation and cellular signaling that could lead to pulmonary fibrosis. In this study, we investigated the fibrogenic responses induced by CeO₂ in a rat model at various time points up to 84 days post-exposure. Male Sprague Dawley rats were exposed to CeO₂ by a single intratracheal instillation. Alveolar macrophages (AM) were isolated by bronchial alveolar lavage (BAL). AM-mediated cellular responses, osteopontin (OPN) and transform growth factor (TGF)- β 1 in the fibrotic process were investigated. The results showed that CeO₂ exposure significantly increased fibrotic cytokine TGF- β 1 and OPN production by AM above controls. The collagen degradation enzymes, matrix metalloproteinase (MMP)-2 and -9 and the tissue inhibitor of MMP were markedly increased in the BAL fluid at 1 day- and subsequently declined at 28 days after exposure, but remained much higher than the controls. CeO₂ induced elevated phospholipids in BAL fluid and increased hydroxyproline content in lung tissue in a dose- and time-dependent manner. Immunohistochemical analysis showed MMP-2, MMP-9 and MMP-10 expressions in fibrotic regions. Morphological analysis noted increased collagen fibers in the lungs exposed to a single dose of 3.5 mg/kg CeO₂ and euthanized at 28 days post-exposure. Collectively, our studies show that CeO₂ induced fibrotic lung injury in rats, suggesting it may cause potential health effects.

Keywords

Cerium oxide; Nanoparticle; Pulmonary fibrosis; Metalloproteinases; Phospholipidosis

*Corresponding author at: PPRB/HELD, NIOSH, 1095 Willowdale Road, Morgantown, WV 26505-2888, USA. Fax: +1 304 285 5938. jym1@cdc.gov (J.Y. Ma).

Disclaimer

The findings and conclusions in this report have not been formally disseminated by the NIOSH and should not be construed to represent any agency determination or policy.

Conflict of interest

The authors declare that there are no conflicts of interest.

Introduction

Cerium, a member of the lanthanide metals, is very reactive and a strong oxidizing agent that is stabilized when associated with an oxygen ligand. Cerium oxide has been used as a polishing agent for glass mirrors, plate glass, television tubes, ophthalmic lenses, and precision optics. Due to the ability of cerium oxide to donate and store oxygen from their crystal lattices, it has been recently used as a diesel fuel borne catalyst in conjunction with a particulate filter to reduce the ignition temperature of the carbonaceous diesel exhaust particles (DEP), resulting to more efficient burning of DEP and the regeneration of the particulate filter (HEI, 2001; Prospect, 2009). Although cerium oxide substantially decreases both particle mass (>90%) and number (99%) concentrations in the exhaust, a small amount of cerium oxide is emitted in the particulate phase of the exhaust (HEI, 2001). HEI (2001) also reported that cerium measured in emissions was found primarily in the oxide form and in particles less than 0.5 μm in diameter. The health effects of cerium oxide (CeO_2) through pulmonary exposure have not been well established, making cerium oxide nanoparticles in diesel exhaust a possible occupational and environmental health concern.

Occupational exposure to rare earth (RE) metals, of which cerium is the major component (80%), has been shown to induce rare earth pneumoconiosis with pathologic conditions that include granulomas and interstitial fibrosis (McDonald et al., 1995; Sabbioni et al., 1982; Waring and Watling, 1990). A common feature of rare earth pneumoconiosis is the presence of cerium particles in the alveoli and interstitial tissue even in patients whose exposure to cerium had stopped for over 20 years (Pairon et al., 1994). These findings demonstrate that cerium oxide is potentially a noxious fibrotic agent, and the use of cerium compounds in diesel fuel may pose a serious health risk to those exposed to cerium oxide from diesel exhaust in either occupational or environmental settings.

Studies have shown that exposure of rats to cerium oxide induces both pulmonary and systemic toxicity (EPA, 2009; HEI, 2001), and leads to impaired pulmonary clearance of these particles, similar to that observed in rare earth pneumoconiosis in humans exposed to cerium compounds. A previous study carried out in our laboratory demonstrated that exposure of rats to a single intratracheal instillation of cerium oxide nanoparticles induced a sustained pulmonary inflammatory response up to 28 days post-exposure (Ma et al., 2011). The cerium oxide-induced pulmonary responses were characterized by a time-dependent switching of alveolar macrophage (AM) phenotype from the classic activated, inflammatory subset of M1 to the alternatively activated, and fibrogenic subset of M2, as evidenced by increased expression of the M2 marker arginase-1 (Arg-1) (Munder et al., 1998). This indicates that in addition to acute inflammatory lung injury, cerium oxide has a persistent effect in chronic lung injury that may include pulmonary fibrosis.

Pulmonary fibrosis is characterized by an excessive deposition of extracellular matrix in the interstitium, where fibroblasts play a major role in the reconstruction of damaged connective tissue by producing new extracellular matrix (ECM) components. The production of fibrogenic mediators, such as transforming growth factor-beta ($\text{TGF-}\beta$)-1 and osteopontin (OPN) by resident macrophages and fibroblasts induces ECM gene expression and plays a key role in fibroblast activation as seen in silica-induced lung fibrosis (Natoli et al., 1998;

Nau et al., 1997; Scabilloni et al., 2005). OPN is a matricellular protein and functions as a fibrogenic promoter for the migration, adhesion, and proliferation of fibroblasts. The expression of OPN mRNA was significantly increased in cerium oxide-exposed lung tissue as demonstrated in our previous study (Ma et al., 2011). The balance between ECM synthesis and degradation of matrix components is crucial for tissue repair. To preserve such a balance, matrix metalloproteinases (MMPs), which represent a family of extracellular and cell surface-associated proteinases, and their physiological inhibitors, the tissue inhibitors of matrix metalloproteinases (TIMPs), must work together to assure normal lung development and proper wound healing. Abnormal activation of proteolytic and/or anti-proteolytic functions can lead to lung diseases, including fibrosis (Gueders et al., 2006). Indeed, in human idiopathic pulmonary fibrosis (IPF), unregulated fibroblast proliferation and extracellular matrix accumulation have been demonstrated to result from excessively elevated TIMPs compared to MMPs, which leads to a nondegrading fibrillar collagen microenvironment (Selman et al., 2000).

In silica-exposed rat lungs, MMPs were significantly induced (Perez-Ramos et al., 1999; Scabilloni et al., 2005). There was a concurrent increase in collagen synthesis, which ultimately led to nodule formation and lung fibrosis. Bonniaud et al. (2004) have shown that a transient over-expression of the active TGF- β 1 in lungs resulted in significantly higher levels of TIMP-1, and progressive pulmonary fibrosis developed after a longer exposure time. OPN, along with MMP-2 activation, has also been associated with bleomycin-induced fibrosis (Berman et al., 2004; Toya et al., 2010). These studies show that when MMPs and TIMPs are produced in elevated levels modification of the extracellular matrix and initiation of the fibrotic process occur.

Few studies have investigated cerium oxide-induced pulmonary responses (McDonald et al., 1995; Porru et al., 2001; Vocaturo et al., 1983). Serious lung injuries resulting from cerium oxide exposure, such as phospholipidosis (Ma et al., 2011) and alveolar proteinosis (Toya et al., 2010), have been identified in animal models. However, the mediators and mechanisms involving in pulmonary fibrosis have not been characterized. The objective of the current study is to characterize the lung deposition of cerium oxide, the time and dose dependence of cerium oxide-induced pulmonary fibrosis, and the involvement of fibrogenic cytokines and ECM modulators in the development of fibrosis.

Materials and methods

Animal exposures

Specific pathogen-free male Sprague–Dawley (Hla: SD-CVF) rats (~250 g) were purchased from Hilltop Laboratories (Scottsdale, PA). Rats were kept in cages individually ventilated with HEPA-filtered air, housed in an AAALAC-approved facility and provided food and water ad libitum. Animals were used after a 1 week acclimatization period. Cerium oxide nanoparticles, 10 wt.% in water with average diameter at ~20 nm, were obtained from Sigma-Aldrich (St Louis, MO, USA). Cerium oxide samples diluted in saline were used for animal exposures as described previously by Ma et al. (2011). Briefly, rats were anesthetized with sodium methohexital (35 mg/kg, i.p.) and placed on an inclined restraint board. Rats were exposed to 0.3 ml suspensions of cerium oxide (with final concentrations

at 0.15, 0.5, 1.0, 3.5 or 7 mg/kg body weight) via intratracheal instillation. Saline (0.3 ml) was administered to control rats. The treated animals were euthanized at 1-, 3-, 10-, 28- or 84-days post-exposure.

Particle characterization

The primary particle size and size of the particles as instilled in this study have been characterized previously. The diameter of primary cerium oxide particle is in the range of 6.4–14.8 nm with the mean at $9.26 \pm .58$ nm when determined by field emission scanning electron microscopy (FESEM). The diameter of primary particle was also determined in the range of 6.25–17.5 nm with a mean diameter of $10.14 \pm .76$ nm using transmission electron microscopy (TEM) (Nalabotu et al., 2011). We have also reported previously that dynamic light scattering of nanoparticles was diluted in saline for intratracheal instillation. These particles agglomerate in saline, with a major particle peak at 2.5 μ m and a small subset with average size of 0.3 μ m (Ma et al., 2011). The surface area of the particle used is in the range of 80–100 m²/g using BET (Sigma Chemicals). The purity of the cerium oxide samples used in this study has been characterized by Yokel et al. (2009). The sum of the contamination from lead, aluminum, copper, titanium, iron, nickel and zinc was <0.2% of the Ce concentration according to ICP-MS analysis.

Isolation of alveolar macrophages (AM) by bronchoalveolar lavage and AM cultures

Animals were anesthetized with sodium pentobarbital (0.2 g/kg) and exsanguinated by cutting the renal artery. AM were obtained by bronchoalveolar lavage (BAL) with a Ca⁺⁺, Mg⁺⁺-free phosphate-buffered medium (145 mM NaCl, 5 mM KCl, 1.9 mM NaH₂PO₄, 9.35 mM Na₂HPO₄, and 5.5 mM glucose; pH 7.4) as described previously (Ma et al., 2011). Briefly, the lungs were lavaged with 6 ml Ca⁺⁺, Mg⁺⁺-free phosphate-buffered medium in and out twice for the first lavage, and subsequently lavaged with 8 ml of the same buffer for a total of 10 times when a total of 80 ml BAL fluid was collected from each rat. The acellular supernate from the first BAL fluid was saved separately from subsequent lavages for analysis of phospholipids, metalloproteinases (MMPs) and tissue inhibitor for metalloproteinase (TIMP). Cell pellets from each animal were centrifuged and combined, washed, and resuspended in a HEPES-buffered medium (145 mM NaCl, 5 mM KCl, 10 mM HEPES, 5.5 mM glucose, and 1.0 mM CaCl₂; pH 7.4). Cell counts and purity were measured using an electronic cell counter equipped with a cell sizing attachment (Coulter Multisizer III with a 256C channelizer, Beckman Coulter Electronics, Brea, CA).

AM-enriched cells were obtained by adherence of lavaged cells to the tissue culture plate as described previously (Yang et al., 1999). After removal of nonadherent cells, AM were cultured in fresh Eagle Minimum Essential Medium (BioWhittaker, Walkersville, MD) for an additional 24 h. AM-conditioned media were collected, centrifuged, and the supernates were saved in aliquots at –80 °C for further analysis of cytokines.

CytoViva hyperspectral imaging

Sirius red stained tissue was used in the darkfield-based illumination as this aided in differentiation between cerium oxide particles and normal tissue. Nanoparticles in lung tissue were imaged using a high signal-to-noise, darkfield-based illumination on an

Olympus BX-41 microscope (CytoViva, Auburn, AL) at 100× oil immersion. Verification of the particles imaged as cerium oxide nanoparticles was based on using the CytoViva hyperspectral imaging system to capture the spectrum (400–1000 nm) and compared it with spectra from cerium oxide doped standard sections. CytoViva's patented illumination technology, when integrated onto a standard optical microscope, creates a high signal-to-noise, darkfield-based image. The combination of the CytoViva Hyperspectral Imaging and CytoViva Microscope System has been used to quantify the presence of a wide range of nanomaterials in cells and tissue or in composites. The system captures the VNIR (400–1000 nm) spectrum within each pixel of the scanned field of view. Advanced analytical software then provides detailed spectral analysis of the scanned materials.

Measurement of soluble mediators, hydroxyproline, and phospholipids. Transforming growth factor (TGF)- β 1 and osteopontin (OPN)

The activities of TGF- β 1 and OPN were assayed in the AM cultured medium using ELISA kits from R&D Systems (Minneapolis, MN) and Assay Designs (Ann Arbor, MI), respectively. The assays were carried out according to the manufacturer's instructions.

Matrix metalloproteinase (MMP)-2, MMP-9 and tissue inhibitors of metalloproteinase (TIMP)-1

The levels of MMP-2, MMP-9 and TIMP-1 were determined in the first BAL fluid, using ELISA kits from Insight Genomics (Falls Church, VA), Cusabio Biotech Co., LTD. (Wuhan, Hubei, China), and R&D Systems Inc. (Minneapolis, MN), respectively, following the manufacturer's protocols.

Total phospholipids

The amount of total phospholipids in BAL fluid was measured as the phosphorus present in the lipid extracts, which was extracted using chloroform-methanol (2:1, v/v) as described previously (Bartlett, 1959). Phospholipid content was obtained by multiplying lipid phosphorus values by 25 (Oyarzun and Clements, 1978).

Hydroxyproline

The formation of collagen in the lungs was analyzed by measurement of hydroxyproline content in the lung tissues. Rat lungs were chopped and hydrolyzed in 6N HCl for 48–72 h at 110 °C. Hydroxyproline was determined according to the method of Kivirikko et al. (1967).

Microscopic and immunohistochemical methods. Transmission electron microscopy (TEM)

For AM ultrastructure analysis by TEM, cell pellets of BAL cells were fixed in Karnovsky's fixative (2.5% glutaraldehyde+3% paraformaldehyde in 0.1 M sodium cacodylate, pH 7.4) and postfixed with osmium tetroxide. Cells were dehydrated in graded alcohol solutions and propylene oxide and embedded in LX-112 (Ladd, Williston, VT). Ultrathin sections were stained with uranyl acetate and lead citrate and examined under TEM.

Histological examination

Rat lung tissues from different exposure groups were fixed immediately after termination by intratracheal instillation of 10% neutral buffered formalin at a pressure of 30 cm H₂O (at an altitude of 960 ft), embedded in paraffin, and stained with hematoxylin and eosin for light microscopic examinations.

Sirius Red staining for collagen detection

Collagen in the lungs was detected with Sirius Red staining (Junqueira et al., 1979), a quantitative morphometric method for collagen determination in the lungs (Antonini et al., 2000; Malkusch et al., 1995). Paraffin sections were deparaffinized and rehydrated with xylene-alcohol series to distilled water. The slides were then stained with 0.1% Picrosirius solution (100 mg of Sirius Red F3BA in 100 ml of saturated aqueous picric acid, pH 2) for 1–2 h, washed for 1 min in 0.01 N HCl, counterstained with Mayer's hematoxylin for 2 min, dehydrated, and mounted with a coverslip.

Quantitative morphometric analysis

Quantitative morphometric methods were used to measure the average thickness of the fibrillar collagen in the alveolar wall and the extent of collagen formation in the alveolar region. Volume and surface density were measured using standard morphometric analyses (Underwood, 1970). This consisted of basic point and intercept counting. Volume density was determined from counting the number of points over the appropriate structures in a section relative to total alveolar region points. Point categories included: alveolar wall tissue and Sirius Red positive connective tissues in the alveolar regions and points over Sirius Red positive connective tissues. Surface density of the alveolar wall was determined from intercepts between a line overlay and the alveolar wall. These point and intercept counts were made using a 121-point/11-line overlay graticule (12.5 mm square with 100 divisions) at 100× magnification taken at six locations equally spaced across each section (one section per animal). This process was repeated twice for each animal. In order to limit the measurements to alveolar parenchyma, areas containing airways or blood vessels greater than 25 mm in diameter were excluded from the analysis. Average thickness of the fibrillar collagen in the alveolar wall was computed from two times the ratio of volume density of points over fibrillar collagen to the surface density of the alveolar wall. The collagen content of the alveolar walls was computed as the percentage of points over collagen divided by the total points over alveolar tissue.

Immunohistochemistry

Paraffin sections were deparaffinized and rehydrated with xylene-alcohol series to distilled water. Antigen retrieval was according to the method described by Scabilloni et al. (2005). Briefly, slides were placed in 0.01 M citrate buffer solution (pH 6.0), and microwaved at a high setting for 105 s to bring the solution to 100 °C and was maintained at that temperature for an additional 6 min. Sections were then equilibrated to room temperature and rinsed in distilled water. Endogenous peroxidase was blocked by placing the sections in 3% hydrogen peroxide-methanol (1:1 v/v) solution at room temperature for 20 min. After being rinsed in Tris buffer (0.1 M, pH 7.4), the sections were loaded into a Sequenza staining tray

(Shandon-Lipshaw, Pittsburgh, PA), rinsed, and blocked with 1% BSA in PBS for 30 min. After addition of the primary antibody solution, the section was incubated for 16 h at 4 °C; the sections were washed with buffer and incubated with the secondary antibody that was a biotinylated anti-rabbit and anti-mouse immunoglobulin adsorbed to abolish cross-reactivity with serum proteins of the rat (Dako, Carpinteria, CA). The sections were then washed in buffer, incubated with streptavidin peroxidase for 30 min, and again washed with buffer. This antibody complex was detected by incubation with 3,3'-diaminobenzidine tetrahydrochloride (DAB; Zymed Laboratories, San Francisco, CA) for 7 min. After detection, sections were washed with distilled water, counterstained with Mayer's hematoxylin for 1 min, rinsed, dehydrated, and mounted. Primary antibodies for MMP were obtained from NeoMarkers (Fremont, CA) and consisted of antibodies to detect MMP-2 or gelatinase A (Ab-1 mouse monoclonal IgG, 1:100), MMP-9 or gelatinase B (Ab-8 mouse monoclonal IgG, 1:50), MMP-10 or stromelysin-2 (Ab-2 mouse monoclonal IgG, 1:500).

Statistical analyses

Data are presented as means±standard errors. Comparisons were made using analysis of variance (ANOVA) with means testing by Dunnett's test when compared to the controls. A $p < .05$ was considered to be significant.

The histological data were analyzed using analysis of variance (STATGRAF). Bartlett's test was used to test for homogeneity of variances between groups. Statistical differences were determined using one-way analysis of variance (ANOVA) with significance set at $p < 0.05$. When significant F values were obtained, individual means were compared to control using Duncan's multiple comparison procedure (Duncan, 1955) and $p < 0.05$ was considered to be significant. Data are given as mean±SE.

Results

Cerium oxide-induced cellular and acellular mediators

In cerium oxide-exposed AM, significant increases in TGF- β 1 secretion occurred at dose levels of 3.5 and 7 mg/kg equivalent to .875 and 1.75 mg/rat, up to 28 days post-exposure. The production peaked at 3 days post exposure, but remained significantly elevated at 10 days after the cerium oxide exposure (Fig. 1A). At the 1 mg/kg dose, the TGF- β 1 production by AM at different time periods was higher than but not statistically different from that of the controls. The production of the fibrotic cytokine, TGF- β 1, in mouse AM cultured medium has been reported to follow a similar transient pattern (Bonniaud et al., 2004).

The production of OPN by cerium oxide-exposed AM was significantly elevated at 10 and 28 days post-exposure (Fig. 1B), but not at 1 day after exposure (data not shown). There is a decline of OPN measured in AM cultured medium at 28 days after exposure comparing to that obtained at 10 days post-exposure, but OPN was still significantly elevated when compared to the controls. These results show that OPN is secreted by cerium oxide-exposed AM as long as 28 days post exposure. Thus, it may play a significant role in mediating cerium oxide-induced fibrotic lung injury.

The presence of MMP-2, MMP-9 and TIMP-1 in the first BAL fluid in response to cerium oxide exposure is shown in Fig. 2. The results show that there is a dose-dependent induction of these proteolytic and anti-proteolytic enzymes related to ECM remodeling after cerium oxide exposure. The production of these proteolytic and antiproteolytic enzymes at 1 day was higher than at 28 days-post-exposure, however, both enzymes were significantly higher than the control at 1- and 28-days after exposure. Both MMP-2 (Fig. 2A) and MMP-9 (Fig. 2B) are proteolytic enzymes that cause degradation of lung collagen, whereas TIMP-1 (Fig. 2C) binds to MMP-9 to inactivate the enzyme. These results show that there is a general excess of TIMP-1 compared to MMP-9, which may inhibit collagen degradation in ECM.

Phospholipidosis

Pulmonary exposure to cerium oxide resulted in a dose-dependent increase of the PL content in the BAL fluid at 28 and 84 days post exposure (Fig. 3A). The results showed a ~10-fold increase in PL in the cerium oxide (7 mg/kg or 1.75 mg/rat)-exposed lungs (1.5 ± 0.41 mg/ml) over that of the controls (0.14 ± 0.02 mg/ml) at 28 days post exposure. The increased PL content at 84-day exposure period was lower than the 28-day exposure groups, but remained 5 fold higher than the control. Fig. 3C shows a significant increase in the lamellar body filled vacuoles in and around AM isolated from a cerium oxide (3.5 mg/kg)-exposed lung at 10 days after exposure, as revealed by TEM. The corresponding TEM micrograph for the control is given in Fig. 3B. These results demonstrate that exposure of rats to cerium oxide induces pulmonary phospholipidosis similar to that observed in silica-exposed lungs (Ma et al., 1999; Porter et al., 2001).

Localization of cerium oxide particle, MMPs, and TIMP in lung tissue

Fig. 4 shows enhanced darkfield-based illumination of Sirius Red stained lung sections from control and cerium oxide-exposed lungs. Lung tissue appears in various shades of reddish-brown, red blood cells are green, and cerium oxide particles are white. Fig. 4A shows the absence of particles in control lung tissue. At 28 days after exposure of rats to a single intratracheal dose of 7 mg/kg of cerium oxide, illuminated white cerium oxide particles were clearly detected in AM, the interstitium and in the airspace mixed with lung surfactant (Fig. 4B). Representative spectra for cerium oxide particles in the tissue section (upper panel C) and normal tissue (lower panel C) clearly distinguish the particles. Each color in the spectra is from a different point (pixel) of the cerium oxide particles in the tissue section and normal tissue, respectively. The presence of particles in lung tissue is consistent with cerium oxide-induced pulmonary inflammation which showed sustained elevation of PMN infiltration for 28 days at the same dose (Ma et al., 2011).

Immunolocalization of MMP-2-, MMP-9-, MMP-10 and TIMP-1 were demonstrated as brown DAB precipitate in cells in fibrotic regions of the lung at 28 days after a single dose of cerium oxide (7 mg/kg) (Figs. 5B, D, F and H, respectively). The corresponding controls are shown in panels A, C, E and G. In addition to being located in fibrotic regions, MMP-2, MMP-9 and TIMP-1 expressions were as shown in airspace masses of surfactant-cerium oxide (arrow head). PMN were also found in the airspaces. In addition to be in the fibrotic regions of cerium oxide-exposed lungs, MMP-10 (Fig. 5F) was more diffusely distributed throughout the tissue, whereas its expression in saline controls was minimal (Panel E).

Hydroxyproline content in lung tissues and morphometric analysis of lung fibrosis

The cerium oxide-induced fibrosis was determined via measurement of lung hydroxyproline content (Fig. 6A) and quantitative morphometric analysis of lung tissue via Sirius Red staining methods (Figs. 6B, C, and D). Exposure of rats to cerium oxide increased lung hydroxyproline content, a major component of collagen and a marker for fibrosis, in a dose and time-dependent manner (Fig. 6A). Exposure of rats to lower concentrations of cerium oxide (1 mg/kg) significantly increased the hydroxyproline level in the lung tissues at 84 days, but not 28 days post exposure. However, rats exposed to cerium oxide at or above 3.5 mg/kg exhibited significantly increased lung hydroxyproline contents at both 28 and 84 days post-exposure. These data demonstrate that exposure of rats to cerium oxide resulted in a dose- and time-dependent increase of hydroxyproline in the lungs, indicating that cerium oxide exposure induced lung fibrosis.

Morphometric analysis of the lung tissues to detect localized collagen formation via Sirius Red staining showed that cerium oxide exposure, at a single 7 mg/kg intratracheal instillation, induced lung fibrosis at 28 days after exposure (Fig. 6B). Quantitative morphometric analysis of the average thickness of the alveolar wall shows that exposure of rats to higher doses of cerium oxide (3.5 and 7 mg/kg) significantly increased alveolar wall thickness compared to controls (Fig. 6C). Quantitative analysis of collagen volume density, based on the morphometric analysis of Sirius Red stained sections, showed that exposure to cerium oxide (7 mg/kg) significantly increased the collagen content in the alveolar wall, i.e. the volume density of collagen in the alveolar wall of tissues from rats exposed to 7 mg/kg of cerium oxide at 28 days post-exposure was nearly doubled (1.89-fold) of that of the control (Fig. 6D).

Discussion

With increasing usage of cerium oxide in various industrial applications, such as in catalytic combustion of diesel fuels, studies of cerium oxide as an environmental particulate have begun to emerge. Previous studies carried out in our laboratory have shown that exposure of rats to cerium oxide nanoparticles by a single intratracheal instillation (up to 7 mg/kg or 1.75 mg/rat) induced lung inflammation, cytotoxicity, air/capillary damage, and a switch of AM population from the classic, proinflammatory subset M1 to the profibrogenic subset M2 macrophages up to 28 days post exposure. The cerium oxide nanoparticle-induced inflammatory response, which showed persistent influx of PMN for 28 days, was without the presence of granulomas, and the AM were characterized by increased mRNA expression of OPN (Ma et al., 2011). In other studies, cerium oxide nanoparticle exposure has been shown to induce pulmonary inflammation and small granulomas at an intratracheal dose of 34 mg/kg in rats (Toya et al., 2010), and a dose range of 50 to 400 mg/kg in mice (Park et al., 2010). In a recent study, Srinivas et al. (2011) reported that exposure of rats to cerium oxide nanoparticles through head and nose inhalation, at a dose level of 641 mg/m³ for 4 h, induced inflammatory responses in the lung including microgranulomas, impairment of clearance, and chronic inflammation. It is apparent that these studies employed much higher doses than our studies, which may account for the granuloma response. However, all these studies showed that cerium oxide can be toxic to the lungs.

Cerium oxide is considered a fibrotic agent, which has been implicated in studies of rare earth pneumoconiosis (McDonald et al., 1995; Waring and Watling, 1990). However, the mechanisms leading to this disease have not been directly demonstrated. The current study was carried out to characterize the fibrogenic activity of cerium oxide nanoparticles and elucidate mechanism(s) through which cerium oxide induces pulmonary fibrosis. The cerium oxide-exposed lungs were characterized by a significant accumulation of phospholipids, which, as shown by histological analysis, formed many large clumps of acellular material mixed with cerium oxide particles in the alveolar region of the lung. The phospholipidosis is also manifested by marked increase in the formation of lipid vesicles and lamella bodies in AM as revealed by TEM. Phospholipidosis is also characteristic of silica-induced pulmonary fibrosis (Ma et al., 1999). However, the relations between phospholipidosis and fibrosis are incompletely understood. Persistent inflammation has been shown to cause tissue injury and atypical repair, leading to alteration of ECM structure and lung fibrosis (Ma et al., 1999; Scabilloni et al., 2005). Cerium oxide-induced phospholipidosis probably results from impaired AM function that leads to a retardation of phospholipid degradation, since the morphology of type II cells in cerium oxide-exposed lungs was not significantly different from that of the control. It is thus quite possible that phospholipidosis may promote the development of fibrogenic (M2) AM (Ma et al., 2011). Studies have shown that stimulation of pulmonary surfactant synthesis by ambroxol in rats resulted in a shift of AM function from an elastase/anti-elastase balance to increased anti-elastase activity on ECM, suggesting that the internalization of surfactants by AM may induce AM functional changes that further affect ECM stability (Pozzi et al., 1987). Although inflammatory pathways may be responsible for epithelial injury and promotes matrix deposition from matrix synthesizing cells leading to fibrosis, however, recently overwhelming evidence of TGF- β playing an important pathogenic role in IPF, suggesting this cytokine can drive epithelial–mesenchymal transition (EMT), fibroblast-to-myofibroblast differentiation, and is most potent inducer of ECM production (Scotton and Chambers, 2007). Cerium oxide exposure induced lung fibrosis may involve EMT and/or fibroblast proliferation and differentiation, which is under investigation in our laboratory.

Our studies showed that cerium oxide nanoparticle exposure resulted in an increase in lung hydroxyproline content, which is a marker for pulmonary fibrosis. The dose- and time-dependent increase in hydroxyproline further illustrates a fibrotic process resulting from progressive toxicity induced by cerium oxide. Exposure of rats to low concentrations of cerium oxide nanoparticles (1 mg/kg or 0.25 mg/rat) significantly increased the hydroxyproline level in lung tissues obtained at 84 days, but not 28 days, after a single intratracheal dose. However, exposure of rats to cerium oxide at doses of 3.5 mg/kg (or 0.875 mg/rat) and above significantly increased lung hydroxyproline contents at both 28 and 84 days post-exposure. The morphometric analysis of lung tissues for localized collagen formation using Sirius Red staining confirmed the formation of fibrosis in tissue samples obtained from rats exposed to cerium oxide (7 mg/kg or 1.75 mg/rat) at 28 days post-exposure. Quantitatively, it was shown that the connective tissue thickness increased with increasing cerium oxide doses, and the percentage volume density of collagen in the alveolar wall in cerium oxide-exposed lung at 3.5 mg/kg (or 0.875 mg/rat) is nearly doubled over the

control. These results demonstrate that exposure of rats to cerium oxide induces pulmonary fibrosis.

Pulmonary fibrosis resulting from particulate exposure or other insults has been extensively studied, but the detailed mechanisms for initiation and progression remain obscure. In general, the process involves signaling by the host defense system for a classical inflammatory response against the invaders, and, likely a simultaneous response for injury repair. It is known that particle-induced lung inflammation can significantly modify the alveolar microenvironment by activating pro- and anti-inflammatory cytokines and growth factors, and damaging the epithelial barrier. This is of particular significance to cerium oxide exposure because a persistent inflammatory response was demonstrated following a single exposure (Ma et al., 2011). The present study demonstrated the presence of cerium oxide nanoparticles in lung tissue at 28 days after exposure using a high signal-to-noise, darkfield-based illumination method. The cerium oxide particles were localized in the acellular surfactant clumps, AM and the lung interstitium. The persistent presence of cerium oxide in lung tissue may play a central role in lung inflammation, basement membrane damage and fibrosis that is similar to findings in workers suffering from rare earth pneumoconiosis with pathological features of pulmonary fibrosis (Vocaturro et al., 1983).

The results also show that cerium oxide markedly induced AM production of TGF- β 1 and OPN, both of which have been shown to elicit a fibrotic response. OPN is a multifunctional cytokine produced by activated lung cells including AM, fibroblasts and T lymphocytes (Denhardt and Guo, 1993). It promotes fibroblast proliferation, adhesion and chemotaxis in the wound healing process (Liaw et al., 1994; Zohar et al., 2004). Studies of bleomycin-induced lung fibrosis in a mouse model demonstrate that OPN was strongly expressed in AM that accumulated in the fibrotic regions of the lung (Takahashi et al., 2001). The profound effects of TGF- β on epithelial cells and fibroblasts have been studied extensively, including promoting epithelial cell apoptosis (Hagimoto et al., 2002), epithelial-to-mesenchymal transition (Gharaee-Kermani et al., 2009; Willis and Borok, 2007), fibroblast proliferation, and their transformation into myofibroblasts (Scotton and Chambers, 2007).

The TGF- β -mediated fibrogenic responses are also linked to cellular production of MMPs, which are proteolytic enzymes involved in the degradation of ECM collagens. It has been shown that TGF- β induces the secretion and activation of the proteolytic enzymes MMP-2 and MMP-9, and conversely TGF- β can also be activated by a number of proteases, including MMP-2 and MMP-9 (Derynck et al., 2001; Yu and Stamenkovic, 2000).

Immunohistochemistry shows that the expression of MMP-2, MMP-9, MMP-10 and TIMP-1 was localized to fibrotic regions of cerium oxide-exposed lungs. These results suggest that the fibrotic development may be partially due to an imbalanced production of the MMPs and TIMPs, which may result from the persistent stimulation by particles in fibrotic foci (Corbel et al., 2000). Localization of MMP-10 in fibrotic regions of the lung is similar to the findings in silica-induced fibrosis (Scabilloni et al., 2005). However, this protease also was detected in acellular surfactant clumps in the alveolar space in cerium oxide-exposed lungs, but not in the alveolar space of silica-exposed lungs (Scabilloni et al., 2005), suggesting that a soluble form exists and is secreted into the alveolar space.

Our studies showed that cerium oxide exposure significantly increased MMP-2, MMP-9, and TIMP-1 levels in a dose-dependent manner. This induction declined with increasing exposure time, but remained elevated when compared to the control. The much higher level of TIMP-1, the tissue inhibitor of MMP-9, relative to MMP-9 after cerium oxide exposure is in agreement with the general observations that in vivo activity of MMPs is under tight control and is generally expressed in very low amounts, while the concentration of TIMP can far exceed MMPs in tissue and extracellular fluids in order to limit their proteolytic activity to focal pericellular sites. However, the elevated MMP-2 and MMP-9 production may play a role in basement membrane disruption and enhancing fibroblast invasion to the alveolar spaces. The TIMP-1/MMP-9 ratio of 113 and 11 determined at 1- and 28-day, respectively, after 7 mg/kg cerium oxide exposure, compared to the ratio of 23 and 13 in controls, suggests that exposure of rats to cerium oxide altered the normal balance of MMP-9 relative to TIMP-1 in the lung. These findings suggest that imbalance of TIMP-1 and MMP-9 may play an important role in ECM remodeling and development of fibrosis. Increased levels of gelatinases MMP-2 and MMP-9 in epithelial lining fluid, which have been implicated in the development of fibrosis, were also observed in IPF patients (Lemjabbar et al., 1999).

In summary, the present study shows that cerium oxide nanoparticles induce a range of mediators involved in lung tissue remodeling, with an imbalanced production of MMPs and TIMP-1 that favors fibrosis. Previously, we have shown a persistent pulmonary inflammation resulting from cerium oxide exposure, characterized by a sustained infiltration of neutrophils into the alveolar region that lasted through the time when fibrosis develops. The current study further demonstrates the presence of cerium oxide particles in lung tissue, AM and airspace and phospholipidosis that may contribute to the alteration of AM function from the proinflammatory M1 to profibrogenic M2 macrophages capable of initiating a fibrotic responses through production of OPN and TGF- β 1. Collectively, these events suggest a mechanism through which the inflammatory cells at the site of injury, in response to cerium oxide exposure, undergo tissue repair process that results in an imbalanced regulation of ECM collagen formation due to the persistent presence of cerium oxide nanoparticles. This study shows that cerium oxide generated in diesel exhaust emission may pose serious adverse health effects.

Conclusion

This study shows that cerium oxide nanoparticles induce lung injury with the presence of these particles in the lung tissues. Cerium oxide particles activated and converted AM from a proinflammatory to profibrotic subset, induced surfactant accumulation, altered the balance of mediators involved in tissue repair process leading to excess collagen deposit and pulmonary fibrosis. These findings suggest that cerium oxide generated in exhaust emission from diesel engine using cerium fuel additive may pose serious adverse health effects. Future studies to elucidate the mechanisms leading to these toxicological responses to cerium oxide exposure are warranted.

Acknowledgments

We thank Dean Newcomer and Sherri Friend for contributions to the pathological analysis work in this paper.

Abbreviations

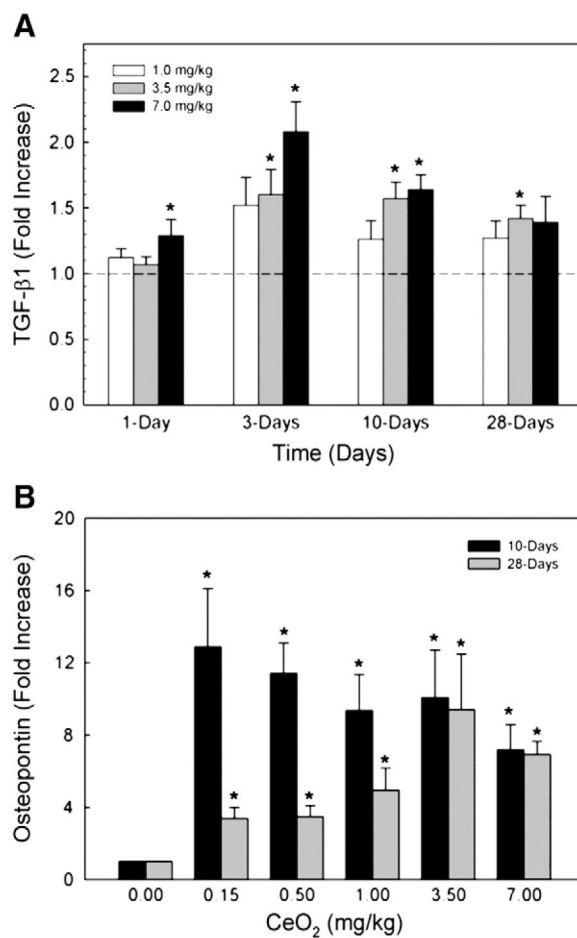
AM	alveolar macrophages
Arg-1	arginase-1
BAL	bronchial alveolar lavage
CeO₂	cerium oxide
DEP	diesel exhaust particles
ECM	extracellular matrix
EMT	epithelial–mesenchymal transition
IPF	idiopathic pulmonary fibrosis
MMP	matrix metalloproteinase
OPN	osteopontin
RE	rare earth
TGF	transform growth factor
TIMP	tissue inhibitors of matrix metalloproteinase
TEM	transmission electron microscopy

References

- Antonini JM, Hemenway DR, Davis GS. Quantitative image analysis of lung connective tissue in murine silicosis. *Exp Lung Res.* 2000; 26:71–88. [PubMed: 10742923]
- Bartlett GR. Phosphorus assay in column chromatography. *J Biol Chem.* 1959; 234:466–468. [PubMed: 13641241]
- Berman JS, Serlin D, Li X, Whitley G, Hayes J, Rishikof DC, Ricupero DA, Liaw L, Goetschkes M, O'Regan AW. Altered bleomycin-induced lung fibrosis in osteopontin-deficient mice. *Am J Physiol Lung Cell Mol Physiol.* 2004; 286(1):L1311–L1318. [PubMed: 14977630]
- Bonnaud P, Kolb M, Galt T, Robertson J, Robbins C, Stampfli M, Lavery C, Margetts PJ, Roberts AB, Gauldie J. Smad3 null mice develop airspace enlargement and are resistant to TGF-beta-mediated pulmonary fibrosis. *J Immunol.* 2004; 173:2099–2108. [PubMed: 15265946]
- Corbel M, Boichot E, Lagente V. Role of gelatinases MMP-2 and MMP-9 in tissue remodeling following acute lung injury. *Braz J Med Biol Res.* 2000; 33:749–754. [PubMed: 10881049]
- Denhardt DT, Guo X. Osteopontin: a protein with diverse functions. *FASEB J.* 1993; 7:1475–1482. [PubMed: 8262332]
- Derynck R, Akhurst RJ, Balmain A. TGF-beta signaling in tumor suppression and cancer progression. *Nat Genet.* 2001; 29:117–129. [PubMed: 11586292]
- Duncan DB. Multiple range and multiple F tests. *Biometrics.* 1955; 11:1–42.
- EPA, U.S. Toxicological Review of Cerium Oxide and Cerium Compounds. 2009. EPA/635/R-08/002F. <http://www.epa.gov/iris/toxreviews/1018tr.pdf>
- Gharaee-Kermani M, Hu B, Phan SH, Gyetko MR. Recent advances in molecular targets and treatment of idiopathic pulmonary fibrosis: focus on TGFbeta signaling and the myofibroblast. *Curr Med Chem.* 2009; 16:1400–1417. [PubMed: 19355895]

- Gueders MM, Foidart JM, Noel A, Cataldo DD. Matrix metalloproteinases (MMPs) and tissue inhibitors of MMPs in the respiratory tract: potential implications in asthma and other lung diseases. *Eur J Pharmacol.* 2006; 533:133–144. [PubMed: 16487964]
- Hagimoto N, Kuwano K, Inoshima I, Yoshimi M, Nakamura N, Fujita M, Maeyama T, Hara N. TGF-beta 1 as an enhancer of Fas-mediated apoptosis of lung epithelial cells. *J Immunol.* 2002; 168:6470–6478. [PubMed: 12055267]
- Health Effects Institute (HEI). HEI Communication. Vol. 9. Integrated Laboratory Systems; Boston, MA, USA: 2001. Evaluation of human health risk from cerium added to diesel fuel.
- Junqueira LCU, Bignolas G, Brentani RR. Picrosirius staining plus polarization microscopy, a specific method for collagen detection in tissue sections. *Histochem J.* 1979; 11:447–455. [PubMed: 91593]
- Kivirikko KI, Laitinen O, Prockop DJ. Modifications of a specific assay for hydroxyproline in urine. *Anal Biochem.* 1967; 19:249–255. [PubMed: 6048697]
- Lemjabbar H, Gosset P, Lechapt-Zalcman E, Franco-Montoya ML, Wallaert B, Harf A, Lafuma C. Overexpression of alveolar macrophage gelatinase B (MMP-9) in patients with idiopathic pulmonary fibrosis: effects of steroid and immunosuppressive treatment. *Am J Respir Cell Mol Biol.* 1999; 20(5):903–913. [PubMed: 10226060]
- Liaw L, Almeida M, Hart CE, Ross R, Schwartz SM, Giachelli CM. Osteopontin promotes vascular cell adhesion and spreading and is chemotactic for smooth muscle cells in vitro. *Circ Res.* 1994; 74:214–224. [PubMed: 8293561]
- Ma JY, Barger MW, Hubbs AF, Castranova V, Weber SL, Ma JK. Use of tetrandrine to differentiate between mechanisms involved in silica-versus bleomycin-induced fibrosis. *J Toxicol Environ Health.* 1999; 57:247–266.
- Ma JY, Zhao H, Mercer RR, Barger M, Rao M, Meighan T, Schwegler-Berry D, Castranova V, Ma JK. Cerium oxide nanoparticle-induced pulmonary inflammation and alveolar macrophage functional change in rats. *Nanotoxicology.* 2011 Oct 6.5:312–325. [PubMed: 20925443]
- Malkusch W, Rehn B, Bruch J. Advantages of sirius red staining for quantitative morphometric collagen measurements in lungs. *Exp Lung Res.* 1995; 21:61–77.
- McDonald JW, Ghio AJ, Sheehan CE, Bernhardt PF, Roggli VL. Rare earth (cerium oxide) pneumoconiosis: analytical scanning electron microscopy and literature review. *Mod Pathol.* 1995; 8:859–865. [PubMed: 8552576]
- Munder M, Eichmann K, Modolell M. Alternative metabolic states in murine macrophages reflected by the nitric oxide synthase/arginase balance: competitive regulation by CD4+ T cells correlates with Th1/Th2 phenotype. *J Immunol.* 1998; 160:5347–5354. [PubMed: 9605134]
- Nalabotu SK, Kolli MB, Triest WE, Ma JY, Manne ND, Katta A, Addagarla HS, Rice KM, Blough ER. Intratracheal instillation of cerium oxide nanoparticles induces hepatic toxicity in male Sprague–Dawley rats. *Int J Nanomedicine.* 2011; 6:2327–2335. [PubMed: 22072870]
- Natoli G, Costanzo A, Guido F, Moretti F, Bernardo A, Burgio VL, Agresti C, Levrero M. Nuclear factor kB-independent cytoprotective pathways originating at tumor necrosis factor receptor-associated factor 2. *J Biol Chem.* 1998; 273:31262–31272. [PubMed: 9813034]
- Nau GJ, Guilfoile P, Chupp GL, Berman JS, Kim SJ, Kornfeld H, Young RA. A chemoattractant cytokine associated with granulomas in tuberculosis and silicosis. *Proc Natl Acad Sci U S A.* 1997; 94:6414–6419. [PubMed: 9177232]
- Oyarzun MJ, Clements JA. Control of lung surfactant by ventilation, adrenergic mediators, and prostaglandins in the rabbit. *Am Rev Respir Dis.* 1978; 117:879–891. [PubMed: 26302]
- Pairon JC, Roos F, Iwatsubo Y, Janson X, Billon-Galland MA, Bignon J, Brochard P. Lung retention of cerium in humans. *Occup Environ Med.* 1994; 51:195–199. [PubMed: 8130849]
- Park EJ, Cho WS, Jeong J, Yi JH, Choi K, Kim Y, Park K. Induction of inflammatory responses in mice treated with cerium oxide nanoparticles by intratracheal instillation. *J Health Sci.* 2010; 56:387–396.
- Perez-Ramos J, de Lourdes Segura-Valdez M, Vanda B, Selman M, Pardo A. Matrix metalloproteinases 2, 9, and 13, and tissue inhibitors of metalloproteinases 1 and 2 in experimental lung silicosis. *Am J Respir Crit Care Med.* 1999; 160:1274–1282. [PubMed: 10508819]

- Porru S, Placidi D, Quarta C, Sabbioni E, Pietra R, Fortaner S. The potencial role of rare earths in the pathogenesis of interstitial lung disease: a case report of movie projectionist as investigated by neutron activation analysis. *J Trace Elem Med Biol.* 2001; 14:232–236. [PubMed: 11396783]
- Porter DW, Ramsey D, Hubbs AF, Battelli L, Ma J, Barger M, Landsittel D, Robinson VA, McLaurin J, Khan A, Jones W, Teass A, Castranova V. Time course of pulmonary response of rats to inhalation of crystalline silica: histological results and biochemical indices of damage, lipidosis, and fibrosis. *J Environ Pathol Toxicol Oncol.* 2001; 20(Suppl 1):1–14. [PubMed: 11570667]
- Pozzi E, Salmona M, Masturzo P, Genghini M, Sceisi M, Spialtini L, Luisetti M. Role of alveolar phospholipids in bleomycin-induced pulmonary fibrosis in the rat. *Respiration.* 1987; 51(Suppl 1): 23–32. [PubMed: 2440083]
- Prospect. Toxicological review of nano cerium oxide. Support of Prospect: Eco-toxicology Test Protocols for Representative Nanomaterials in Support of the OECD Sponsorship Programme. 2009. http://www.nanotechia-prospect.org/managed_assets/files/prospect_nano-ceo2_literature_review.pdf
- Sabbioni E, Pietra R, Gaglione P, Vocaturo G, Colombo F, Zanoni M, Rodi F. Long-term occupational risk of rare-earth pneumoconiosis. A case report as investigated by neutron activation analysis. *Sci Total Environ.* 1982; 26:19–32. [PubMed: 7167813]
- Scabilloni JF, Wang L, Antonini JM, Roberts JR, Castranova V, Mercer RR. Matrix metalloproteinase induction in fibrosis and fibrotic nodule formation due to silica inhalation. *Am J Physiol Lung Cell Mol Physiol.* 2005; 288:L7097–L7717.
- Scotton CJ, Chambers RC. Molecular targets in pulmonary fibrosis: the myofibroblast in focus. *Chest.* 2007; 132(4):1311–1321. [PubMed: 17934117]
- Selman M, Ruiz V, Cabrera S, Segura L, Ramirez R, Barrios R, Pardo A. TIMP-1, -2, -3, and -4 in idiopathic pulmonary fibrosis. A prevailing non-degradative lung microenvironment? *Am J Physiol Lung Cell Mol Physiol.* 2000; 279:L562–L574. [PubMed: 10956632]
- Srinivas A, Rao PJ, Selvam G, Murthy PB, Reddy PN. Acute inhalation toxicity of cerium oxide nanoparticles in rats. *Toxicol Lett.* 2011; 205:105–115. [PubMed: 21624445]
- Takahashi F, Takahashi K, Okazaki T, Maeda K, Ienaga H, Maeda M, Kon S, Uede T, Fukuchi Y. Role of osteopontin in the pathogenesis of bleomycin-induced pulmonary fibrosis. *Am J Respir Cell Mol Biol.* 2001; 24:264–271. [PubMed: 11245625]
- Toya T, Takata A, Otaki N, Takaya M, Serita F, Yoshida K, Kohyama N. Pulmonary toxicity induced by intratracheal instillation of coarse and fine particles of cerium dioxide in male rats. *Ind Health.* 2010; 48:3–11. [PubMed: 20160402]
- Underwood, EE. *Quantitative Stereology.* Addison-Wesley; Reading, MA: 1970.
- Vocaturo G, Colombo F, Zanoni M, Rodi F, Sabbioni E, Pietra R. Human exposure to heavy metals. Rare earth pneumoconiosis in occupational workers. *Chest.* 1983; 83:780–783. [PubMed: 6839821]
- Waring PM, Watling RJ. Rare earth deposits in a deceased movie projectionist. A new case of rare earth pneumoconiosis? *Med J Aust.* 1990; 153:726–730. [PubMed: 2247001]
- Willis BC, Borok Z. TGF-beta-induced EMT: mechanisms and implications for fibrotic lung disease. *Am J Physiol Lung Cell Mol Physiol.* 2007; 293:L525–L534. [PubMed: 17631612]
- Yang HM, Barger MW, Castranova V, Ma JK, Yang JJ, Ma JY. Effects of diesel exhaust particles (DEP), carbon black, and silica on macrophage responses to lipopolysaccharide: evidence of DEP suppression of macrophage activity. *J Toxicol Environ Health.* 1999; 58:261–278.
- Yokel RA, Florence RL, Unrine JM, Tseng MT, Graham UM, Wu P, Grulke EA, Sultana R, Hardas SS, Butterfield DA. Biodistribution and oxidative stress effects of a systemically-introduced commercial ceria engineered nanomaterial. *Nanotoxicology.* 2009; 3(3):234–248.
- Yu Q, Stamenkovic I. Cell surface-localized matrix metalloproteinase-9 proteolytically activates TGF-beta and promotes tumor invasion and angiogenesis. *Genes Dev.* 2000; 14:163–176. [PubMed: 10652271]
- Zohar R, Zhu B, Liu P, Sodek J, McCulloch CA. Increased cell death in osteopontin-deficient cardiac fibroblasts occurs by a caspase-3-independent pathway. *Am J Physiol Heart Circ Physiol.* 2004; 287:H1730–H1739. [PubMed: 15165989]

**Fig. 1.**

Cerium oxide exposure induced TGF- β 1 and OPN in AM culture medium. AM were isolated by bronchoalveolar lavage and cultured at 37 °C for 24 h. TGF- β 1 (A) and OPN (B) levels were measured in the cultured supernate using ELISA. The values are expressed as means \pm SE, n=6. *Significantly different from saline controls, p<0.05. The dotted line indicates control.

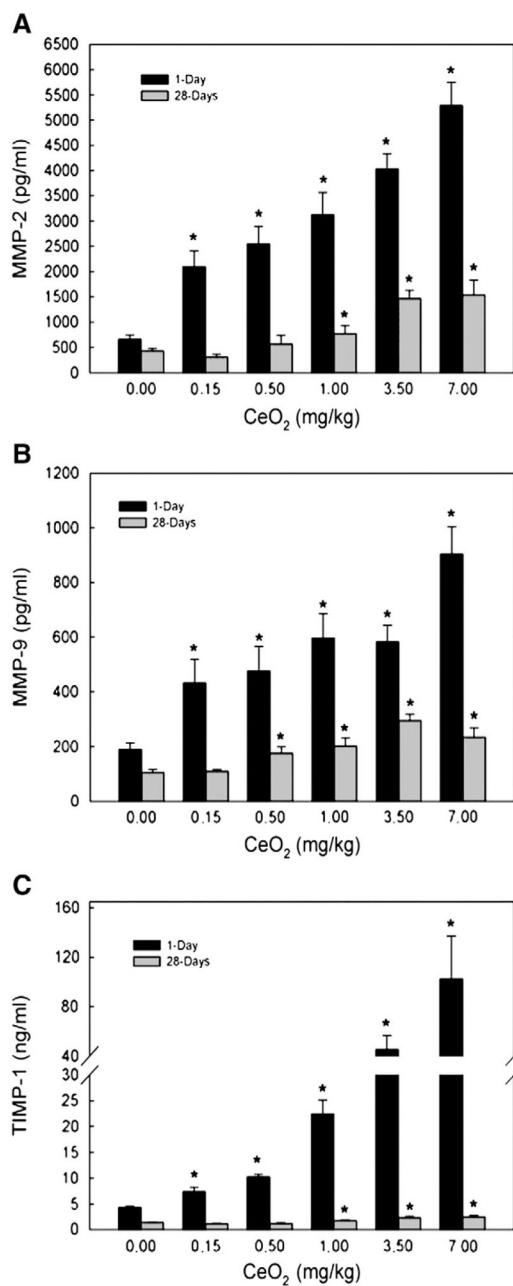


Fig. 2. MMP-2, MMP-9 and TIMP-1 levels in the first BAL fluid monitored at 1- and 28-day post CeO₂ exposure. The first BAL fluid was isolated from saline and CeO₂-exposed rats, as described in the Materials and methods section. The MMPs and TIMP levels were determined using ELISA. The values are expressed as means±SE, n=6. *Significantly different from saline control group at p<0.05.

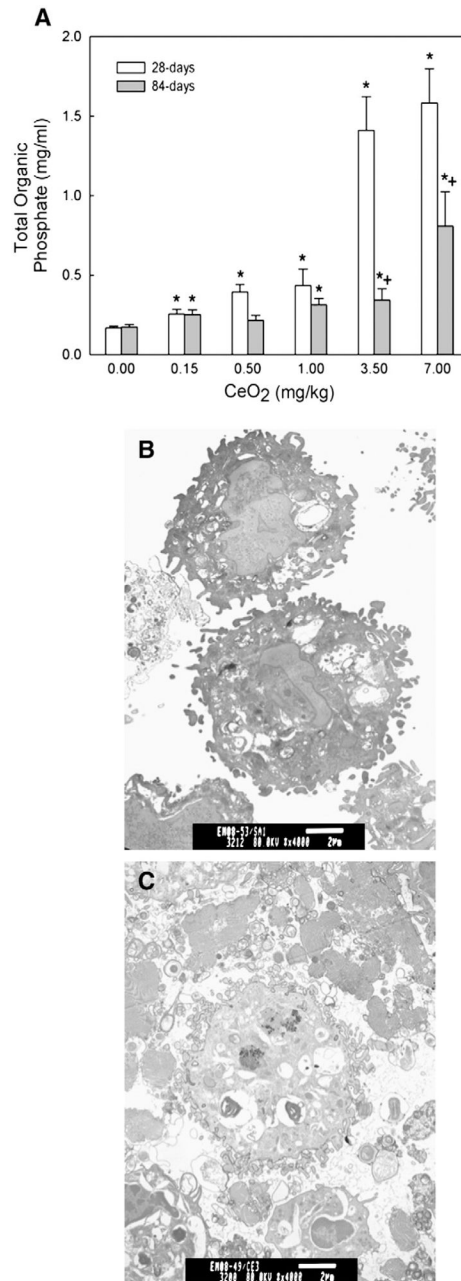


Fig. 3. Effect of CeO₂ exposure on phospholipids content in the BAL fluid and micrographs of TEM analysis of AM. (A) The phospholipid content in the first BAL fluids obtained from saline and various concentrations of CeO₂-exposed rats at 28 and 84 days post exposure. TEM of AM isolated by bronchoalveolar lavage from (B) control and (C) CeO₂ (3.5 mg/kg)-exposed rats at 10 days post-exposure. (Bar=2 μm). The values are expressed as means± SE, n=6. *Significantly different from saline control group at p<0.05. +Significantly different from 28-day exposure groups, at p<0.05.

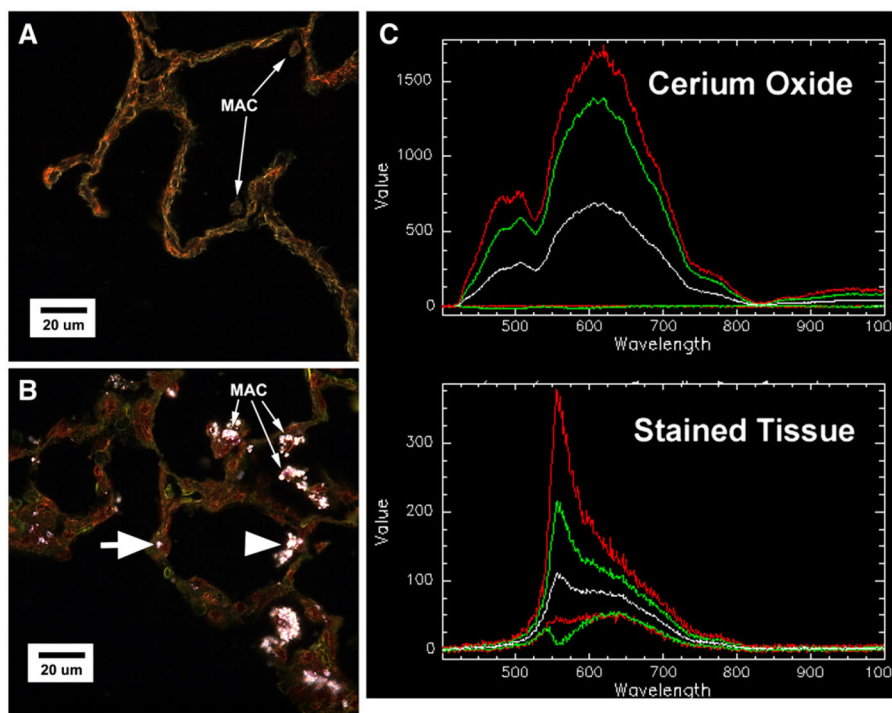


Fig. 4. Cerium oxide particles in lung tissue and pulmonary fibroblasts isolated from CeO₂ (a single intratracheal dose of 7 mg/kg)-exposed rats, at 28 days post exposure. Control lung tissues exhibit no particles under high resolution, dark field illumination (A). Illuminated CeO₂ particles, using darkfield-based illumination, were clearly detected in macrophages (MAC), the interstitium (arrow), in acellular surfactant clumps (arrow head), in the airspace as free particles (B). Panel C gives representative intensity versus wavelength spectra of points (pixels) of CeO₂ particles in the cerium oxide-exposed tissue section (upper panel) and spectra of control tissue. Each different colored curve represents a different point. Small arrow: MAC; big arrow: interstitium; Arrow head: acellular mass of surfactant-cerium oxide in the air space.

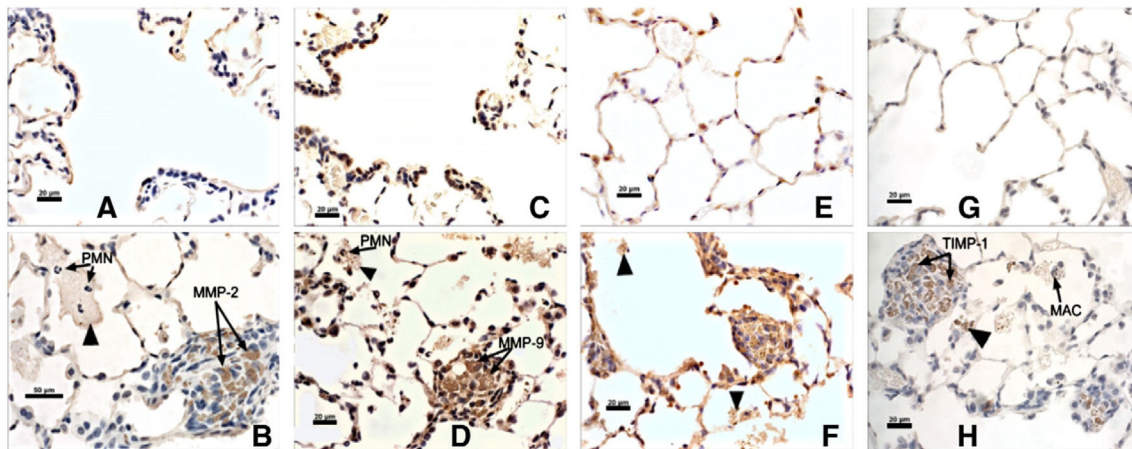


Fig. 5. Immunohistochemical localization of MMP-2, -9, -10 and TIMP-1 in lung tissues. Exposure of rats to cerium oxide at 28 days after a single intratracheal instillation of 7 mg/kg of cerium oxide. Lungs were isolated and treated as described in the Materials and methods section. Representative immunolocalization for MMP-2, MMP-9, MMP-10 and TIMP-1 (brown-DAB precipitate) of saline control lung sections is shown in the upper panels (Panels A, C, E and G) and corresponding cerium oxide-treated lung sections in the lower panels (Panels B, D, F and H). MMP-2, MMP-9, and TIMP-1 (Panels B, D and H) were intensely expressed in cells of fibrotic areas in CeO₂-exposed lung, respectively. MMP-10 (Panel F) was intensely expressed in fibrotic areas of CeO₂-exposed lungs and was also expressed diffusely throughout the lungs. MMP-10 expression in saline controls was minimal (Panel E). Arrow head: acellular mass of surfactant-cerium oxide in the air space, containing PMN (small arrows).

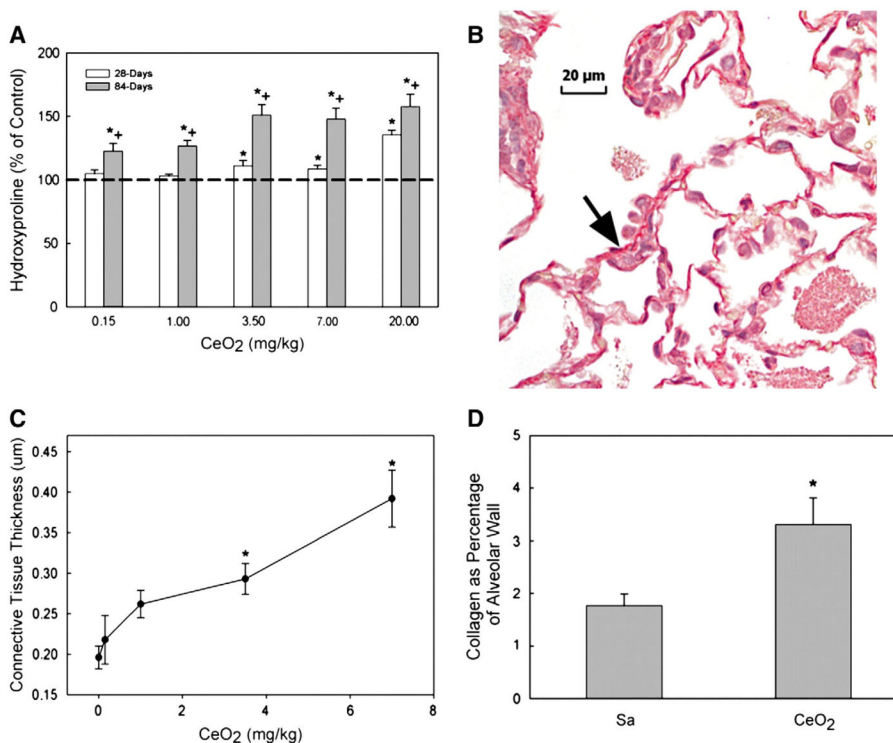


Fig. 6. Hydroxyproline content and Sirius red staining for collagen in the lung tissue and quantitative morphometric analysis of alveolar wall thickness and collagen fiber volume in CeO₂ exposed rat lungs. (A) Lung tissues exposed to various levels of CeO₂ at 28 and/or 84 days after exposure. Hydroxyproline content in the lung tissues was monitored as described in the Materials and methods section. The values are expressed as means±SE, n=6. (B) Light micrograph of Sirius red staining for collagen formation in the lung tissues (arrow) at 28 days post exposure (cerium dose: 7 mg/kg). (C) Quantitative analysis of dose-dependent increase in the thickness of alveolar wall connective tissue. (D) Quantitative analysis of collagen volume expressed as a percentage of total tissue volume, based on the morphometric analysis of Sirius Red stained sections. *Significantly different from saline controls; p<0.05. +Significantly different from 28-day exposure groups, at p<0.05.